

Current-induced motion of a transverse magnetic domain wall in the presence of spin Hall effect

Soo-Man Seo, Kyoung-Whan Kim, Jisu Ryu, Hyun-Woo Lee, and Kyung-Jin Lee

Citation: *Appl. Phys. Lett.* **101**, 022405 (2012); doi: 10.1063/1.4733674

View online: <http://dx.doi.org/10.1063/1.4733674>

View Table of Contents: <http://apl.aip.org/resource/1/APPLAB/v101/i2>

Published by the [American Institute of Physics](http://www.aip.org).

Related Articles

Strain induced magnetic domain evolution and spin reorientation transition in epitaxial manganite films
Appl. Phys. Lett. **101**, 022411 (2012)

Influence of the winding number on field- and current driven dynamics of magnetic vortices and antivortices
J. Appl. Phys. **112**, 013917 (2012)

Domain-related origin of magnetic relaxation in compressively strained manganite thin films
Appl. Phys. Lett. **101**, 012408 (2012)

Asymmetric Pt/Co/Pt-stack induced sign-control of current-induced magnetic domain-wall creep
Appl. Phys. Lett. **100**, 262408 (2012)

Superferromagnetism and coercivity in Co-Al₂O₃ granular films with perpendicular anisotropy
J. Appl. Phys. **111**, 123915 (2012)

Additional information on *Appl. Phys. Lett.*

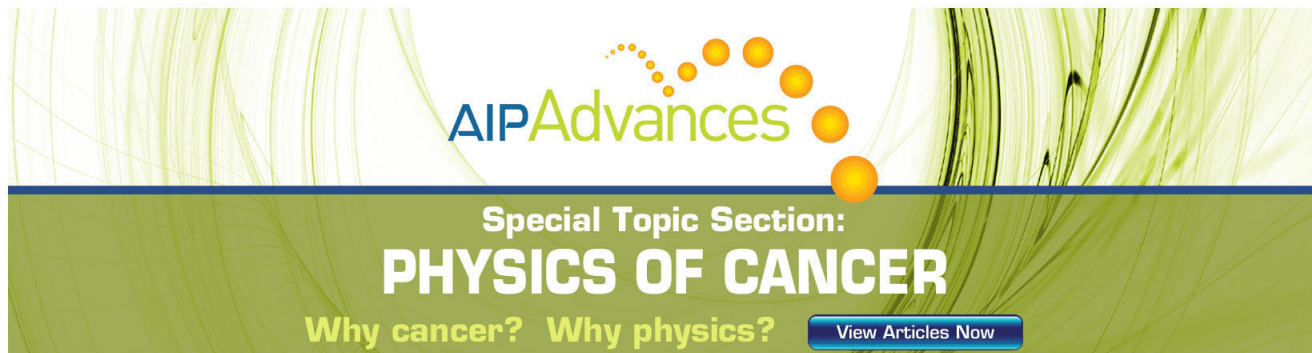
Journal Homepage: <http://apl.aip.org/>

Journal Information: http://apl.aip.org/about/about_the_journal

Top downloads: http://apl.aip.org/features/most_downloaded

Information for Authors: <http://apl.aip.org/authors>

ADVERTISEMENT



AIP Advances

Special Topic Section:
PHYSICS OF CANCER

Why cancer? Why physics? [View Articles Now](#)

Current-induced motion of a transverse magnetic domain wall in the presence of spin Hall effect

Soo-Man Seo,^{1,a)} Kyoung-Wan Kim,^{2,a)} Jisu Ryu,² Hyun-Woo Lee,^{2,b)} and Kyung-Jin Lee^{1,3,4,c)}

¹Department of Materials Science and Engineering, Korea University, Seoul 136-701, Korea

²PCTP and Department of Physics, Pohang University of Science and Technology, Kyungbuk 790-784, Korea

³Center for Nanoscale Science and Technology, National Institute of Standards and Technology, Gaithersburg, Maryland 20899-8412, USA

⁴Maryland Nanocenter, University of Maryland, College Park, Maryland 20742, USA

(Received 13 January 2012; accepted 21 June 2012; published online 9 July 2012)

We theoretically study current-induced dynamics of a transverse magnetic domain wall in bi-layer nanowires consisting of a ferromagnetic layer on top of a nonmagnetic layer with strong spin-orbit coupling. Domain wall dynamics is characterized by two threshold current densities, J_{th}^{WB} and J_{th}^{REV} , where J_{th}^{WB} is a threshold for the chirality switching of the domain wall and J_{th}^{REV} is another threshold for the reversed domain wall motion caused by spin Hall effect. Domain walls with a certain chirality may move opposite to the electron-flow direction with high speed in the current range $J_{th}^{REV} < J < J_{th}^{WB}$ for the system designed to satisfy the conditions $J_{th}^{WB} > J_{th}^{REV}$ and $\alpha > \beta$, where α is the Gilbert damping constant and β is the nonadiabaticity of spin torque. Micromagnetic simulations confirm the validity of analytical results. © 2012 American Institute of Physics. [<http://dx.doi.org/10.1063/1.4733674>]

Electric manipulation of domain walls (DWs) in magnetic nanowires can be realized by the spin-transfer torque (STT) due to the coupling between local magnetic moments of the DW and spin-polarized currents.^{1,2} Numerous studies on this subject have addressed its fundamental physics,³⁻⁵ and explored its potential application towards data storage and logic devices.⁶ Up until now, however, most studies have focused on the effect of the spin current that is polarized by a ferromagnetic layer.

Another way to generate a spin current is the spin Hall effect (SHE).^{7,8} In ferromagnet (FM)/nonmagnet (NM) bi-layer systems, an in-plane charge current density (J_c) passing through the NM is converted into a perpendicular spin current density (J_s) owing to the SHE. The ratio of J_s to J_c is parameterized by spin Hall angle. This spin current caused by SHE exerts a STT (=SHE-STT) on the FM and consequently modifies its magnetization dynamics. During the last decade, most studies on the SHE have focused on measuring the spin Hall angle.⁹⁻¹⁴ Recently the magnetization switching^{15,16} and the modulation of propagating spin waves by SHE-STT were investigated.¹⁷⁻¹⁹ However, the effect of SHE-STT on current-induced DW dynamics has not been examined.

In this letter, we study the DW dynamics in a nanowire consisting of FM/NM bi-layers (Fig. 1(a)), where FM has an in-plane magnetic anisotropy and NM has strong spin-orbit coupling (SOC) responsible for the SHE. All current-induced STTs are included in our study. A charge current passing through the FM generates conventional adiabatic and nonadiabatic STTs,²⁰⁻²² whereas a charge current flowing through the NM experiences SHE and generates SHE-

STT on the FM. For the current running in the x axis, the modified Landau-Lifshitz-Gilbert equation including all the STTs is given by

$$\frac{\partial \mathbf{m}}{\partial t} = -\gamma \mathbf{m} \times \mathbf{H}_{\text{eff}} + \alpha \mathbf{m} \times \frac{\partial \mathbf{m}}{\partial t} - b_J \mathbf{m} \times \left(\mathbf{m} \times \frac{\partial \mathbf{m}}{\partial x} \right) - \beta b_J \mathbf{m} \times \frac{\partial \mathbf{m}}{\partial x} - \theta_{SH} c_J \mathbf{m} \times (\mathbf{m} \times \hat{y}), \quad (1)$$

where \mathbf{m} is the unit vector along the magnetization, α is the Gilbert damping constant, b_J ($= g\mu_B P J_F / 2eM_S$) is the magnitude of adiabatic STT, β is the nonadiabaticity of STT, $\theta_{SH} c_J$ ($= \theta_{SH} \gamma \hbar J_N / 2eM_S t_F$) is the magnitude of SHE-STT, θ_{SH} is an effective spin Hall angle for the bi-layer system, γ is the gyromagnetic ratio, g is the Landé g -factor, μ_B is the Bohr magneton, P is the spin polarization in the FM, e is the electron charge, M_S is the saturation magnetization of the FM, and J_F (J_N) is the current density in the FM (NM). J_F and J_N are determined by a simple circuit model, i.e., $J_F = J_0(t_F + t_N)\sigma_F / (t_F\sigma_F + t_N\sigma_N)$ and $J_N = J_0(t_F + t_N)\sigma_N / (t_F\sigma_F + t_N\sigma_N)$, where J_0 is the average current density in the bi-layer nanowire, σ_F (σ_N) is the conductivity of the FM (NM), and t_F (t_N) is the thickness of the FM (NM) layer. We assume that θ_{SH} is smaller than 1 as is usually the case experimentally.

For a nanowire with an in-plane magnetic anisotropy, a net effective field is given by

$$\mathbf{H}_{\text{eff}} = \frac{2A}{M_S} \frac{\partial^2 \mathbf{m}}{\partial x^2} + H_K m_x \hat{x} + \mathbf{H}_d, \quad (2)$$

where A is the exchange stiffness constant, H_K is the easy axis anisotropy field along the x axis, and \mathbf{H}_d is the magneto-static field given by $\mathbf{H}_d(\mathbf{r}) = M_S \int d^3 r' \tilde{N}(\mathbf{r} - \mathbf{r}') \mathbf{m}(\mathbf{r}')$, where the components of the tensor \tilde{N} are given by

^{a)}S.-M. Seo and K.-W. Kim contributed equally to this work.

^{b)}Electronic mail: hwl@postech.ac.kr.

^{c)}Electronic mail: kj_lee@korea.ac.kr.

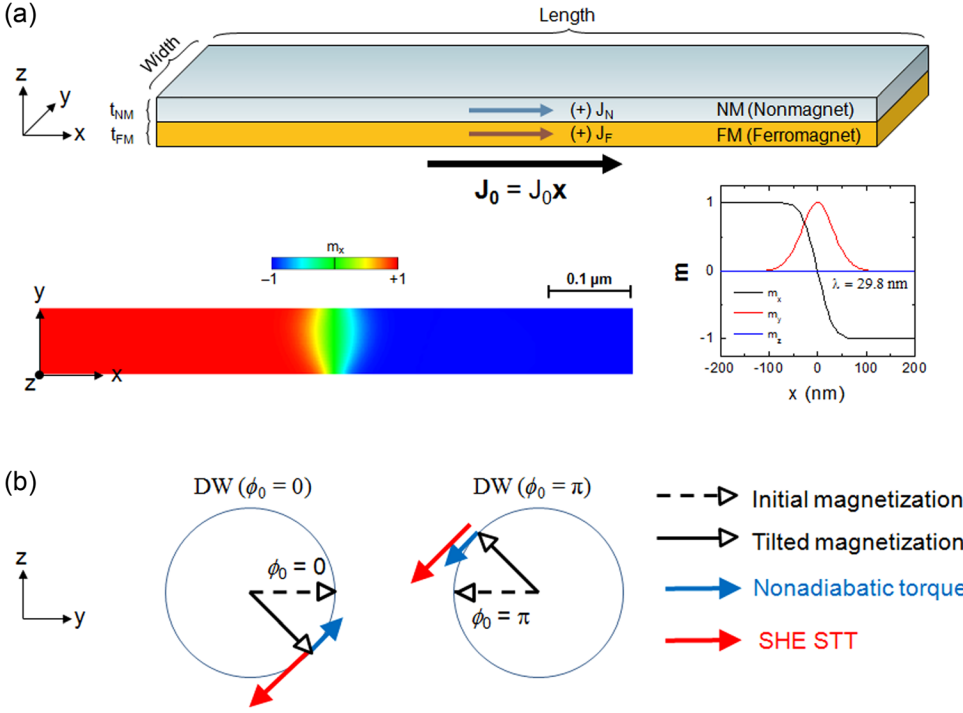


FIG. 1. (a) Schematics of FM/NM bilayer nanowire. (Top) Structure. (Lower left) Spatial profile of DW. The colored contour shows x component of the magnetization for 2-D micromagnetics. (Lower right) Width-averaged magnetization components. (b) Schematic illustration of the SHE-STT and the nonadiabatic torque acting on the magnetization at the center of DW, electrons move in $+x$ direction.

$N_{xx} = -[1 - 3x^2/|\mathbf{r}|^2]/|\mathbf{r}|^3$, $N_{xy} = 3xy/|\mathbf{r}|^5$.²³ Other components are defined in a similar way. For a one-dimensional DW as shown in Fig. 1(a), the spatial profile of the magnetization is described by $\mathbf{m} = (\cos\theta, \sin\theta\cos\phi, \sin\theta\sin\phi)$, where $\sin\theta = \text{sech}[(x-X)/\lambda]$, $\cos\theta = -\tanh[(x-X)/\lambda]$, $X(t)$ is the DW position, $\phi(t)$ is the DW tilt angle, and λ is the DW width. The chirality of DW is characterized by the initial DW tilt angle ($\phi_0 = 0$ or π). By using the procedure developed by Thiele,²⁴ we obtain the equations of motion for the two collective coordinates X and ϕ in the rigid DW limit,

$$-\frac{\partial X}{\partial t} + \alpha\lambda\frac{\partial\phi}{\partial t} = b_J - \frac{\gamma H_d \lambda}{2} \sin(2\phi), \quad (3)$$

$$\lambda\frac{\partial\phi}{\partial t} + \alpha\frac{\partial X}{\partial t} = -\beta_{\text{eff}} b_J, \quad (4)$$

where $H_d = (2K_d/M_S)$, $\beta_{\text{eff}} = \beta(1 + B_{SH}\lambda\sin\phi)$, $B_{SH} = \pi\theta_{SH}J_N/2\beta t_F P J_F$, and K_d is the hard-axis anisotropy energy density. From Eqs. (3) and (4), one finds that the effect of SHE-STT on DW dynamics is captured by replacing β by β_{eff} . Assuming that FM is Permalloy (Py: Ni₈₀Fe₂₀) and NM is Pt, for the parameters of $t_F = 4$ nm, $t_N = 3$ nm, $\sigma_F = \sigma_N$, $\theta_{SH} = 0.1$, $\beta \approx 0.01$ to 0.03 ,²⁵ $P = 0.7$, and $\lambda = 30$ nm, we find $B_{SH}\lambda \approx 18$ to 56 , which is not small. Therefore, β_{eff} can be much larger than β unless $\sin\phi$ is extremely small. Furthermore, it is possible that β_{eff} is even negative if $B_{SH}\lambda\sin\phi < -1$.

To get an insight into the effect of SHE-STT on DW dynamics, we derive several analytical solutions from Eqs. (3) and (4). It is known that DW dynamics in a nanowire can be classified into two regimes, i.e., below and above the Walker breakdown.²⁶ Below the Walker breakdown, ϕ increases in the initial time stage from the initial tilt angle $\phi_0 = 0$ or π and becomes saturated to a steady state value. In this limit ($\partial\phi/\partial t = 0$ as $t \rightarrow \infty$), we obtain

$$b_J = \frac{\gamma\alpha H_d \lambda \sin 2\phi}{2(\alpha - \beta_{\text{eff}})}. \quad (5)$$

Threshold adiabatic STT for the Walker breakdown (b_J^{WB}) is obtained from the maximum value of the right-hand-side of Eq. (5), i.e., $b_J^{WB} = \max[\gamma\alpha H_d \lambda \sin 2\phi / 2(\alpha - \beta_{\text{eff}})]$. Note that b_J^{WB} is not simply $[\gamma\alpha H_d \lambda / 2(\alpha - \beta_{\text{eff}})]$ because β_{eff} includes the dynamic variable ϕ . When $B_{SH} = 0$, Eq. (5) reduces to $b_J^{WB} = \gamma\alpha H_d \lambda / 2(\alpha - \beta)$, reproducing the previous result²⁷ in the absence of SHE.

For $|b_J| < |b_J^{WB}|$ (below the Walker breakdown), the DW velocity (v_{DW}) becomes $v_{DW} = -(\beta_{\text{eff}}/\alpha)b_J$, where the value β_{eff} (or $\sin\phi$) is fixed by Eq. (5). Using the small-angle approximation ($\cos\phi \approx \cos\phi_0 = \pm 1$), one finds $\lambda\sin\phi = \pm(\alpha - \beta)b_J / [\gamma\alpha H_d \pm \beta b_J B_{SH}]$, which leads to

$$v_{DW} = -\frac{\beta}{\alpha} b_J \left(1 \pm B_{SH} \frac{(\alpha - \beta)b_J}{\gamma\alpha H_d \pm \beta b_J B_{SH}} \right). \quad (6)$$

Note that v_{DW} depends on the initial tilt angle ϕ_0 . Mathematically, this ϕ_0 dependence of v_{DW} arises since the steady state value of $\sin\phi$ depends on ϕ_0 . Physically, it originates from the fact that SHE-STT acts like a damping or an anti-damping term depending on ϕ_0 . Figure 1(b) shows the schematic illustrations of the nonadiabatic torque (indicated by a blue arrow with solid head) and the SHE-STT (indicated by a red arrow with solid head) in the y - z plane at the center of DW. Here, we assume that electrons flow in $+x$ direction. Let us first consider the case without SHE-STT. For both cases of DW chirality ($\phi_0 = 0$ and π), the magnetization at the center of DW tilts clockwise due to the combined effect of all the torques except the SHE-STT, i.e., the magnetization tilts from its initial direction (indicated by a dotted arrow with hollow head) to a tilted direction (indicated by a solid arrow with hollow head). Then, let us turn on SHE-

STT. For $\phi_0 = 0$, the direction of the nonadiabatic STT is opposite to that of the SHE-STT. Therefore, the DW can move against the electron-flow when the SHE-STT overcomes the nonadiabatic STT. On the contrary, for $\phi_0 = \pi$, the directions of the nonadiabatic STT and the SHE-STT are the same. In this case, thus, the DW always moves along the electron-flow direction. We also remark that for $\phi_0 = 0$, the SHE-STT tends to increase $|\sin\phi|$, thereby enhancing the magnitude of the SHE-STT. Thus, for $\phi_0 = 0$, the SHE-STT is expected to lower the Walker breakdown threshold current density. For $\phi_0 = \pi$, on the other hand, the SHE-STT tends to decrease $|\sin\phi|$, thereby suppressing the magnitude of the SHE-STT. In this case, the decrease of the Walker breakdown threshold current density is not expected.

In a special case with $\beta = \alpha$, $v_{DW} = -b_J$ so that v_{DW} does not depend on SHE-STT. However, this condition is hardly realized in the bi-layer system that we consider since the strong SOC in NM increases the intrinsic α of FM through the spin pumping effect.²⁸ When $B_{SH} = 0$, $v_{DW} = -(\beta/\alpha)b_J$, consistent with the DW velocity in the absence of SHE.²⁷ Note that in our sign convention, a negative b_J corresponds to the electron-flow in $+x$ direction and a positive v_{DW} corresponds to the DW motion along the electron-flow direction. Therefore, when the term in the parenthesis of Eq. (6) is negative, the DW moves against the electron-flow direction instead of along it. Threshold adiabatic STT for this reversed DW motion (b_J^{REV}) is given by

$$b_J^{REV} = \mp \frac{\gamma H_d}{B_{SH}}. \quad (7)$$

For $|b_J| \gg |b_J^{WB}|$ (far above the Walker breakdown), the time-averaged values of $\sin\phi$ and $\sin 2\phi$ can be set to zero because of the precession of ϕ . In this limit, v_{DW} is determined by Eq. (3) and becomes $-b_J$ so that the DW moves along the electron-flow direction and its motion does not depend on SHE-STT.

Based on the above investigations, there are two interesting effects of SHE on current-induced DW dynamics. First, current-induced DW dynamics is determined by two thresholds, b_J^{WB} and b_J^{REV} . When $|b_J^{REV}| < |b_J| < |b_J^{WB}|$, the DW can move against the electron-flow direction. Note that the existence of such b_J range implicitly assumes $|b_J^{REV}| < |b_J^{WB}|$. When this inequality is not satisfied, the DW always moves along the electron-flow direction. For all cases, $|v_{DW}|$ can be larger than $|\beta b_J/\alpha|$ depending on the parameters (see Eq. (6)). Second, v_{DW} is asymmetric against the initial tilt angle ϕ_0 for a fixed current polarity. A similar argument is also valid for a fixed ϕ_0 but with varying the current polarity, i.e., v_{DW} is asymmetric with respect to the current polarity for a fixed ϕ_0 . Therefore, although the condition of $|b_J^{REV}| < |b_J| < |b_J^{WB}|$ is satisfied, the reversed DW motion is expected to be observed only for one current polarity.

To verify the analytical results, we perform a one-dimensional micromagnetic simulation by numerically solving Eq. (1). We consider a Py/Pt bi-layer nanowire of (length \times width \times thickness) = (2000 nm \times 80 nm \times 4 nm (Py) and 3 nm (Pt)) (Fig. 1(a)). Py material parameters of $M_S = 800$ kA/m, $A = 1.3 \times 10^{-11}$ J/m, $P = 0.7$, $\alpha = 0.02$, and

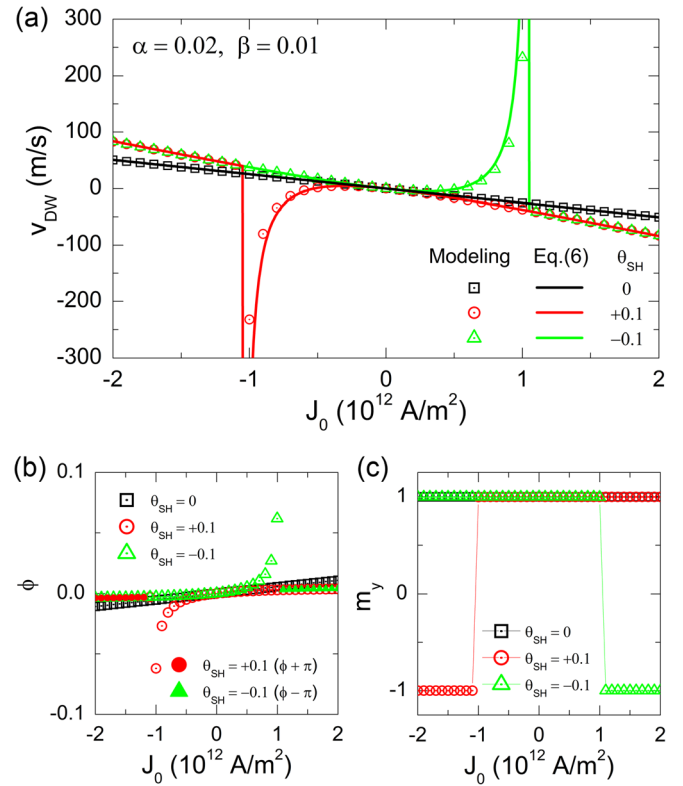


FIG. 2. Domain wall velocity for $\alpha > \beta$. (a) DW velocity (v_{DW}) as a function of the total current density of bi-layer (J_0) for three values of θ_{SH} ($=+0.1, 0.0, -0.1$) and $\beta = 0.01$ ($\alpha = 0.02$). Symbols are modeling results, whereas solid lines correspond to Eq. (6). (b) DW tilt angle (ϕ) as a function of J_0 . Filled symbols above the chiral switching threshold ($|J_0| = 1.1 \times 10^{12}$ A/m²) are shifted from their original values by $-\pi$ (filled green triangles) and $+\pi$ (filled red circles). (c) Normalized y component of the magnetization at the DW center (m_y) as a function of J_0 .

$\beta = 0.01$ to 0.03 are used. The crystalline anisotropy and the temperature are assumed to be zero. Conductivities of both layers are assumed to be the same as $\sigma_{Py} = \sigma_{Pt} = 6.5$ ($\mu\Omega\text{m}$)⁻¹, and thus $J_0 = J_F = J_N$. For all cases, the initial DW tilt angle ϕ_0 is set to zero.

Analytical and numerical results are compared in Fig. 2. DW velocity (v_{DW}) and DW tilt angle (ϕ) as a function of the total current density of the bi-layer (J_0) for three values of θ_{SH} ($=+0.1, 0.0, -0.1$) and $\beta = 0.01$ (thus $\alpha > \beta$) are shown in Figs. 2(a) and 2(b), respectively. v_{DW} is estimated from the terminal velocity. Here, we test both positive and negative values of θ_{SH} since the spin Hall angle can have either sign.¹⁶

Current dependences of v_{DW} (Fig. 2(a)) and ϕ (Fig. 2(b)) show close correlation, meaning that the DW tilting plays a crucial role for the effect of SHE on DW dynamics as demonstrated analytically. In Fig. 2(a), the numerical results (symbols) are in agreement with the results obtained from Eq. (6) (lines). For $\theta_{SH} = 0$, v_{DW} is linearly proportional to J_0 and the DW always moves along the electron-flow direction. However, for $0.5 \times 10^{12} \leq J_0 \leq 1.0 \times 10^{12}$ A/m² with $\theta_{SH} = -0.1$ (-1.0×10^{12} A/m² $\leq J_0 \leq -0.5 \times 10^{12}$ A/m² with $\theta_{SH} = 0.1$), v_{DW} has the same sign as the current. Thus, the DW moves along the current-flow direction for these ranges of the current. The threshold for the reversed DW motion is consistent with the analytical solution of Eq. (7), i.e., $b_J^{REV} = \pm 26.6$ m/s corresponding to $J_0 = \pm 0.52 \times 10^{12}$ A/m². The maximum v_{DW}

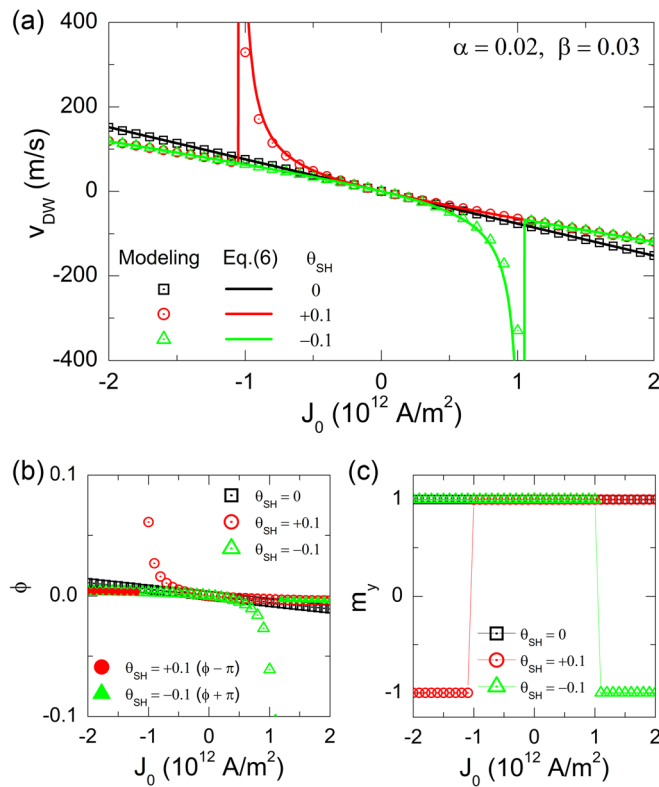


FIG. 3. Domain wall velocity for $\alpha < \beta$. (a) DW velocity (v_{DW}) as a function of the total current density of bi-layer (J_0) for three values of θ_{SH} ($=+0.1, 0.0, -0.1$) and $\beta = 0.03$ ($\alpha = 0.02$). Symbols are modeling results, whereas solid lines correspond to Eq. (6). (b) DW tilt angle (ϕ) as a function of J_0 . Filled symbols represent the cases that the chirality of DW switches from its initial tilt angle $\phi_0 = 0$. (c) Normalized y component of the magnetization at the DW center (m_y) as a function of J_0 .

is obtained at $J_0 = \pm 1.0 \times 10^{12}$ A/m 2 immediately before the DW experiences Walker breakdown and switches its chirality. As shown in the Fig. 2(c), the normalized y-component of the magnetization at the DW center (m_y) abruptly changes from ± 1 to ∓ 1 for $J_0 = \pm 1.0 \times 10^{12}$ A/m 2 and $\theta_{SH} = \mp 0.1$. This current density is consistent with the threshold for Walker breakdown (b_J^{WB}), i.e., $b_J^{WB} = \pm 53$ m/s corresponding to $J_0 = \pm 1.045 \times 10^{12}$ A/m 2 . At this current density, v_{DW} is enhanced by a factor of 5 compared to the case for $\theta_{SH} = 0$.

Figs. 3(a) and 3(b) show v_{DW} and ϕ as a function of J_0 for three values of θ_{SH} ($=+0.1, 0.0, -0.1$) and $\beta = 0.03$ (thus $\alpha < \beta$). Similar to the cases for $\beta = 0.01$, v_{DW} is closely correlated to ϕ and significantly enhanced near b_J^{WB} . In this case, in contrast to the case for $\alpha > \beta$, reversed DW motion is not observed. It is because the sign of the $(\alpha - \beta)$ term in Eq. (6) is negative in this case, and thus the overall sign of v_{DW} corresponds to the DW motion along the electron-flow direction. We find that the current-induced Oersted field has only a negligible effect on v_{DW} (not shown). Thus, the numerical results confirm the validity of the analytical solutions; the DW moves along the current-flow direction at the limited range of the current (i.e., $|b_J^{REV}| < |b_J| < |b_J^{WB}|$) when $\alpha > \beta$. In addition, this reversed DW motion appears only for one current polarity.

Finally, we remark the effect of SHE on DW dynamics in the nanowire with a perpendicular anisotropy. It was experimentally reported that the DW moves along the current-flow direction with a high v_{DW} (≈ 400 m/s) in the

perpendicularly magnetized nanowire consisting of Pt/Co/AlO $_x$.^{29,30} We note that this DW dynamics cannot be explained by the SHE only. Considering the materials parameters in Ref. 30 as $M_S = 1090$ kA/m, $K = 1.2 \times 10^6$ J/m 3 , $A = 1.3 \times 10^{-11}$ J/m, $\alpha = 0.2$, $P = 0.7$, $\lambda = 5$ nm, and assuming $\theta_{SH} = 0.1$ and $\beta = 0.1$, we find $B_{SH}\lambda = 18.8$ that is comparable to the value for the Py/Pt bi-layer tested in this work. For Pt/Co/AlO $_x$, however, b_J^{REV} and b_J^{WB} are, respectively, -1.5 and -3 m/s (corresponding to $J_0 = -0.4 \times 10^{11}$ and -0.8×10^{11} A/m 2). These thresholds are much smaller than those of the Py/Pt bi-layer since H_d of DW in a perpendicular system is smaller than in an in-plane system (i.e., $H_d = 848$ mT for the system of Py/Pt in this work, 33 mT for the system in Ref. 30).²³ Note that the maximum DW velocity moving along the current-flow direction (v_{DW}^{REV}) is obtained at $b_J = b_J^{WB}$. The $b_J^{WB} (= -3$ m/s) in Pt/Co/AlO $_x$ system is too small to allow such a high v_{DW}^{REV} (≈ -400 m/s). Indeed, the numerically obtained maximum v_{DW}^{REV} is -8.2 m/s at $J_0 = -0.71 \times 10^{11}$ A/m 2 ($b_J = -2.64$ m/s) (not shown), which is much smaller than the experimentally obtained value, -400 m/s. More importantly, in the Pt/Co/AlO $_x$ system, the reversed DW motion was observed at both current polarities,³¹ whereas the SHE allows the reversed motion at only one current polarity. On the other hand, we theoretically demonstrated that the DW dynamics reported in Refs. 29 and 30 can be explained by STTs caused by Rashba SOC.³² We also remark that one of us reported the effect of SOC on current-driven DW motion recently.³³ In Ref. 33, however, the effect of SOC within FM was investigated, in contrast to the present work where the effect of SOC in NM of the FM/NM bi-layer system is investigated.

To conclude, we present the analytical model for current-induced DW motion in the presence of SHE. We demonstrate that DW dynamics is significantly affected by the SHE. In particular, for the case of $\alpha > \beta$, the SHE enables the reversed DW motion with high speed at one current polarity when the system is designed to satisfy the condition of $|b_J^{REV}| < |b_J^{WB}|$ and the current density is selected to be in the range between the two thresholds. Our result demonstrates that the engineering of SOC and thus the SHE provides an important opportunity for an efficient operation of spintronic devices.

This work was supported by the NRF (2010-0014109, 2010-0023798, 2011-0009278, 2011-0028163, 2011-0030790) and the MKE/KEIT (2009-F-004-01). K.J.L. acknowledges support under the Cooperative Research Agreement between the University of Maryland and the National Institute of Standards and Technology Center for Nanoscale Science and Technology, Award 70NANB10H193, through the University of Maryland.

¹J. C. Slonczewski, *J. Magn. Magn. Mater.* **159**, L1 (1996).

²L. Berger, *Phys. Rev. B* **54**, 9353 (1996).

³A. Yamaguchi, T. Ono, S. Nasu, K. Miyake, K. Mibu, and T. Shinjo, *Phys. Rev. Lett.* **92**, 077205 (2004).

⁴M. Yamanouchi, D. Chiba, F. Matsukura, and H. Ohno, *Nature (London)* **428**, 539 (2004).

⁵M. Kläui, C. A. F. Vaz, J. A. C. Bland, W. Wernsdorfer, G. Faini, E. Cambril, L. J. Heyderman, F. Nolting, and U. Rüdiger, *Phys. Rev. Lett.* **94**, 106601 (2005).

⁶S. S. P. Parkin, M. Hayashi, and L. Thomas, *Science* **320**, 190 (2008).

- ⁷J. E. Hirsch, *Phys. Rev. Lett.* **83**, 1834 (1999).
- ⁸S. Zhang, *Phys. Rev. Lett.* **85**, 393 (2000).
- ⁹S. O. Valenzuela and M. Tinkham, *Nature (London)* **442**, 176 (2006).
- ¹⁰T. Kimura, Y. Otani, T. Sato, S. Takahashi, and S. Maekawa, *Phys. Rev. Lett.* **98**, 156601 (2007).
- ¹¹K. Ando, S. Takahashi, K. Harii, K. Sasage, J. Ieda, S. Maekawa, and E. Saitoh, *Phys. Rev. Lett.* **101**, 036601 (2008).
- ¹²T. Seki, Y. Hasegawa, S. Mitani, S. Takahashi, H. Imamura, S. Maekawa, J. Nitta, and K. Takahashi, *Nature Mater.* **7**, 125 (2008).
- ¹³O. Mosendz, J. E. Pearson, F. Y. Fradin, G. E. W. Bauer, S. D. Bader, and A. Hoffman, *Phys. Rev. Lett.* **104**, 046601 (2010).
- ¹⁴L. Liu, T. Moriyama, D. C. Ralph, and R. A. Buhrman, *Phys. Rev. Lett.* **106**, 106602 (2011).
- ¹⁵L. Liu, O. J. Lee, T. J. Gudmundsen, D. C. Ralph, and R. A. Buhrman, e-print arXiv:1110.6884v2.
- ¹⁶L. Liu, C.-F. Pai, Y. Li, H. W. Tseng, D. C. Ralph, and R. A. Buhrman, *Science* **336**, 555 (2012).
- ¹⁷V. E. Demidov, S. Urazhdin, E. R. J. Edwards, M. D. Stiles, R. D. Michael, and S. O. Demokritov, *Phys. Rev. Lett.* **107**, 107204 (2011).
- ¹⁸Z. Wang, Y. Sun, M. Wu, V. Tiberkevich, and A. Slavin, *Phys. Rev. Lett.* **107**, 146602 (2011).
- ¹⁹E. Padrón-Hernández, A. Azevedo, and S. M. Rezende, *Appl. Phys. Lett.* **99**, 192511 (2011).
- ²⁰G. Tatara and H. Kohno, *Phys. Rev. Lett.* **92**, 086601 (2004).
- ²¹S. Zhang and Z. Li, *Phys. Rev. Lett.* **93**, 127204 (2004).
- ²²A. Thiaville, Y. Nakatani, J. Miltat, and Y. Suzuki, *Europhys. Lett.* **69**, 990 (2005).
- ²³S.-W. Jung, W. Kim, T.-D. Lee, K.-J. Lee, and H.-W. Lee, *Appl. Phys. Lett.* **92**, 202508 (2008).
- ²⁴A. A. Thiele, *Phys. Rev. Lett.* **30**, 230 (1973).
- ²⁵K. Sekiguchi, K. Yamada, S.-M. Seo, K.-J. Lee, D. Chiba, K. Kobayashi, and T. Ono, *Phys. Rev. Lett.* **108**, 017203 (2012).
- ²⁶N. L. Schryer and L. R. Walker, *J. Appl. Phys.* **45**, 5406 (1974).
- ²⁷A. Mougín, M. Cormier, J. P. Adam, P. J. Metaxas, and J. Ferré, *Europhys. Lett.* **78**, 57007 (2007).
- ²⁸Y. Tserkovnyak, A. Brataas, and G. E. Bauer, *Phys. Rev. Lett.* **88**, 117601 (2002).
- ²⁹T. A. Moore, I. M. Miron, G. Gaudin, G. Serret, S. Auffret, B. Rodmacq, A. Schul, S. Pizzini, J. Vogel, and M. Bonfim, *Appl. Phys. Lett.* **93**, 262504 (2008); **95**, 179902 (2009).
- ³⁰I. M. Miron, T. Moore, H. Szabolics, L. D. Buda-Prejbeanu, S. Auffret, B. Rodmacq, S. Pizzini, J. Vogel, M. Bonfim, A. Schul, and G. Gaudin, *Nature Mater.* **10**, 189 (2011).
- ³¹I. M. Miron, private communication (2012).
- ³²K.-W. Kim, S.-M. Seo, J. Ryu, K.-J. Lee, and H.-W. Lee, *Phys. Rev. B* **85**, 180404(R) (2012).
- ³³A. Manchon and K.-J. Lee, *Appl. Phys. Lett.* **99**, 022504 (2011); **99**, 229905 (2011).